

Robust AC Quantum Spin Hall Effect without Participation of Edge States

W. Y. Deng¹, H. Geng¹, Wei Luo¹, Wei Chen², L. Sheng^{1,3}, D. N. Sheng⁴, and D. Y. Xing^{1,3}

¹ National Laboratory of Solid State Microstructures and Department of Physics, Nanjing University, Nanjing 210093, China

² College of Science, Nanjing University of Aeronautics and Astronautics, Nanjing 210016, China

³ Collaborative Innovation Center of Advanced Microstructures, Nanjing University, Nanjing 210093, China

⁴ Department of Physics and Astronomy, California State University, Northridge, California 91330, USA

(Dated: September 17, 2021)

The quantum spin Hall (QSH) effect in the DC regime, which has been intensively researched, relies on the existence of symmetry-protected edge states. Here, we demonstrate that a QSH system behaves quite differently in response to an applied AC electric field, and put forward the idea of AC QSH effect. The AC QSH effect can occur in the bulk without involving the fragile edge states, hence being robust against time-reversal symmetry breaking and disorder. It lays a more solid foundation for practical applications of the two-dimensional topological insulators, in the emerging field of AC spintronics.

PACS numbers: 72.25.-b, 73.43.-f, 73.20.At, 73.50.-h

In recent years, there has been a great surge of research interest in topological insulators (TIs) [1–11]. Two-dimensional TIs, also called quantum spin Hall (QSH) systems [1–3], are featured with a bulk band gap around the Fermi level and gapless helical edge states traversing the band gap. The topological distinction between the QSH materials and ordinary insulators can be described by an unconventional topological invariant, i.e., the Z_2 index [12] or spin Chern number [13–15]. While the existence of edge states in the QSH systems is attributable to the nontrivial bulk band topology, the gapless nature of the edge states is protected by the time-reversal (TR) symmetry [1–3]. The QSH effect provides a purely electrical means to generate dissipationless and noiseless spin current and spin accumulations, and so is promising for applications in high-precision low-power spintronic devices.

Most existing research works about the QSH effect focus on the steady states in the DC regime. In a steady state in the DC regime, only electrons at the Fermi level can contribute to the electronic transport, as indicated clearly by the Landauer-Büttiker formalism, so that the DC QSH effect must be carried by the symmetry-protected gapless edge states that pass through the Fermi level. In the presence of TR-symmetry-breaking perturbations, the edge states become gapped [1–3] and can be localized by any weak disorder due to their one-dimensional nature, according to the textbook theory of Anderson localization. As a consequence, the DC QSH effect is fragile in realistic environments, where such symmetry-breaking perturbations are often unavoidable. So far, conductance near the predicted quantized value through edge channels has been realized only in small samples of HgTe quantum wells [16] and InAs/GaSb bilayers [17], with sizes of the order of $1\mu\text{m} \times 1\mu\text{m}$, and the conductance is strongly suppressed for larger samples. This is in contrast to the conventional quantum Hall effect, for which precisely integer-quantized Hall conduc-

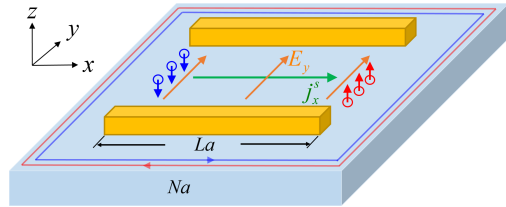


FIG. 1: Proposed experimental setup, and illustration of the AC QSH effect discovered in this Letter. Two metal bars are deposited on the surface of a QSH sample, keeping enough distances from the sample edges. By applying an AC bias voltage to the metal bars, an AC electric field $E_y(t) = E_0 \cos \omega t$ is created along the y direction in the region between the bars (biased region). In response, an AC spin current is generated in the x direction within the biased region, which in turn results in opposite measurable spin accumulations, oscillating with time, near the right and left edges of the biased region. The whole transport process does not involve the edge states.

tivity has been observed in a large variety of materials on the macroscopic scale. The instability of the DC QSH effect remains to be a serious technical barrier to its practical applications.

Recently, AC spin current in the G-Hz frequency range generated through spin pumping has been detected experimentally, which stimulates the emerging field of AC spintronics [18]. In an AC electric field, a QSH system will always be in a transient state, which may display quite different characteristics from the steady state in the DC regime. In this Letter, we demonstrate that the AC QSH effect is much more stable than its DC counterpart. It can occur in the bulk of a QSH material without involving the fragile edge states, if the driving AC electric field is applied only to an inner region of the sample (as illustrated in Fig. 1). We perform exact finite-size numerical calculations, adopting the BHZ model [19] for the QSH effect, based on the Kubo linear-response theory. We show that when electron spin is conserved, a quantized transverse AC spin current is generated within

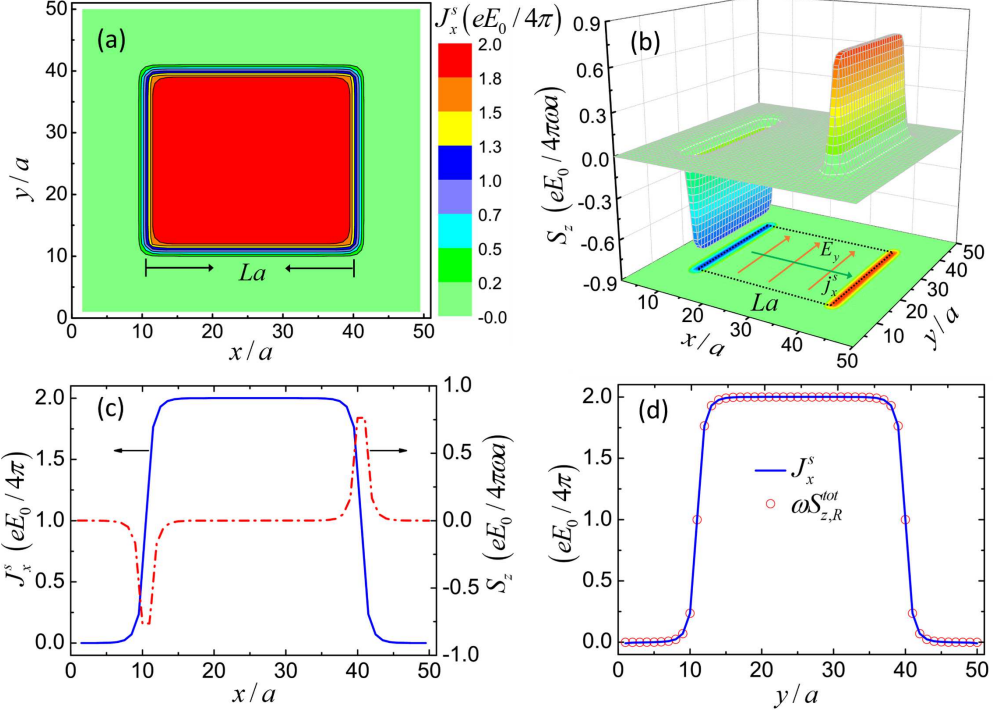


FIG. 2: (a) Profile of spin current density $J_x^s(x, y)$ in the whole sample. (b) Density of spin accumulation $S_z(x, y)$ in the whole sample. (c) Spin current density and density of spin accumulation along the mirror line $y = \frac{Na}{2}$ as functions of x/a . (d) Spin accumulation rate $\omega S_{z,R}^{\text{tot}}(y)$ and spin current density $J_x^s(\frac{Na}{2}, y)$ as functions of y . The sizes of the sample and biased region are set to $N = 50$ and $L = 30$, respectively. The other parameters are taken to be $\hbar\omega = 0.05$, and the Fermi energy $E_F = 0$, in the middle of the band gap.

the region of the electric field (biased region), and measurable spin accumulations, oscillating with time, occur near the transverse edges of the biased region, as required by the spin conservation law. Moreover, even when magnetic disorder is present, breaking both spin conservation and TR symmetry, the spin accumulations remain robust, although the spin current becomes ill-defined. The AC QSH effect lays a more solid foundation for practical applications of the two-dimensional TIs in spintronics, immune to symmetry breaking and disorder.

To study the AC QSH effect numerically, we adopt the lattice version of the BHZ model [19], which can be constructed on a square lattice from the continuum Hamiltonian [19] through the replacements $k_x \rightarrow a^{-1} \sin(k_x a)$, $k_y \rightarrow a^{-1} \sin(k_y a)$ and $k^2 \rightarrow 2a^{-2}[2 - \cos(k_x a) - \cos(k_y a)]$ with a as the lattice constant. After a reverse Fourier transformation, the Hamiltonian in real space is obtained as

$$H_0 = \sum_{\mathbf{r}} c_{\mathbf{r}}^\dagger \varepsilon_0 c_{\mathbf{r}} + \sum_{\mathbf{r}} (c_{\mathbf{r}}^\dagger t_x c_{\mathbf{r}+a\hat{x}} + \text{h.c.}) + \sum_{\mathbf{r}} (c_{\mathbf{r}}^\dagger t_y c_{\mathbf{r}+a\hat{y}} + \text{h.c.}), \quad (1)$$

where $\mathbf{r} = (x, y)$ are the coordinates of a lattice site, and $c_{\mathbf{r}} = (c_{\mathbf{r}\uparrow}, c_{\mathbf{r}\uparrow}, c_{\mathbf{r}\downarrow}, c_{\mathbf{r}\downarrow})$ are the electron annihilation operators on site \mathbf{r} with \uparrow and \downarrow as spin in-

dices and s and p representing two orbits. Here, $\varepsilon_0 = -4(D - B\sigma_z)a^{-2} - M_0\sigma_z$, $t_x = (D - B\sigma_z)a^{-2} - i(2a)^{-1}A\sigma_x s_z$, and $t_y = (D - B\sigma_z)a^{-2} + i(2a)^{-1}A\sigma_y$. $\boldsymbol{\sigma} = (\sigma_x, \sigma_y, \sigma_z)$ and $\mathbf{s} = (s_x, s_y, s_z)$ are the Pauli matrices for orbit and spin, respectively, and A , B , D and M_0 are the parameters of the BHZ model [19]. The topological properties of the model can be described by the topological invariant, spin Chern number, given by $C_s = \text{sgn}(B) + \text{sgn}(M_0)$ [20]. Since C_s is independent of D , without loss of generality, we set $D = 0$ in the following calculations. The Dirac mass M_0 (assumed to be positive) is taken as the unit of energy. The other model parameters are set to $A/a = 3$, and $B/a^2 = 1.5$. For this set of parameters, the BHZ model is in the QSH phase with $C_s = 2$.

We consider a square sample of size Na with open boundary. To demonstrate the independence of the AC QSH effect on the edge states, it is assumed that an AC electric field $E_y(t) = E_0 \cos(\omega t)$ is applied along the y direction in a smaller concentric square region of size La , as illustrated in Fig. 1. We study first the ideal case, where electron spin is conserved. The Kubo linear-response theory [21] is employed to calculate the spin current density $j_x^s(x, y; t)$ and density of spin accumulation $\rho_s(x, y; t)$ induced by the applied electric field. We find that the spin current and spin accumulations are always polar-

ized in the z direction. Besides, for sufficiently large La , the longitudinal component of the spin current along the y direction is negligible, essentially because the system has an insulating gap around the Fermi level. The spin current response to the driving AC electric field is immediate, and so synchronized with the electric field, i.e., $j_x^s(x, y; t) = J_x^s(x, y) \cos(\omega t)$, where $J_x^s(x, y)$ is obtained from the Kubo formula [21] as

$$J_x^s(x, y) = \frac{\hbar^2 e E_0}{a^2} \sum_{m \neq n} \frac{\text{Im}[\langle m | v_y | n \rangle \langle n | v_x^s | m \rangle]}{(E_m - E_n)^2 - (\hbar\omega)^2} f(E_m). \quad (2)$$

Here, the eigenstates $|m\rangle$ with eigenenergies E_m are obtained through exact diagonalization of the Hamiltonian H_0 of the sample, $f(E)$ is the Fermi distribution function, $v_y = \frac{i}{\hbar} [H_0, y]$ is the velocity operator in the biased region, and $v_x^s = \frac{1}{2} \{v_x, s_z\}$ represents the spin velocity operator at (x, y) .

In Fig. 2(a), we show the profile of the calculated spin current density $J_x^s(x, y)$ for a small frequency in the whole sample. We can see that inside the biased region, the ratio $J_x^s(x, y)/E_0 \equiv j_x^s(x, y; t)/E_y(t)$, being equivalent to the frequency-dependent spin Hall conductivity, takes an integer-quantized value 2 in units of the spin conductivity quantum $\frac{e}{4\pi}$, which is well consistent with the spin Chern number $C_s = 2$. The spin current density $J_x^s(x, y)$ vanishes quickly crossing the right and left edges of the biased region. The discontinuities in $J_x^s(x, y)$ imply that electron spins are accumulating or depleting near the edges.

The density of spin accumulation is related to the spin current density through the spin conservation law

$$\frac{\partial \rho_s}{\partial t} + \frac{d j_x^s}{d x} = 0. \quad (3)$$

It follows that the density of spin accumulation is an integral over time of the gradient of the spin current density, and thus lags the spin current by $\pi/2$. As a result, $\rho_s(x, y; t) = S_z(x, y) \sin(\omega t)$, where $S_z(x, y)$ can be obtained from the Kubo formula [21] as

$$S_z(x, y) = \frac{\hbar e E_0}{\omega a^2} \sum_{m \neq n} (E_m - E_n) \times \frac{\text{Re}[\langle m | v_y | n \rangle \langle n | s_z | m \rangle]}{(E_m - E_n)^2 - (\hbar\omega)^2} f(E_m). \quad (4)$$

Here, s_z stands for the Pauli matrix for electron spin at (x, y) . In Fig. 2(b), we plot the calculated profile of the density of spin accumulation in the whole sample. Indeed, there are spin accumulations sharply peaked at the right and left edges of the biased region. In Fig. 2(c), the spin current density and density of spin accumulation along the mirror line $y = \frac{Na}{2}$ as functions of x/a are plotted. One can see more clearly that the peaks of the spin accumulations correspond to the discontinuities in the spin current density.

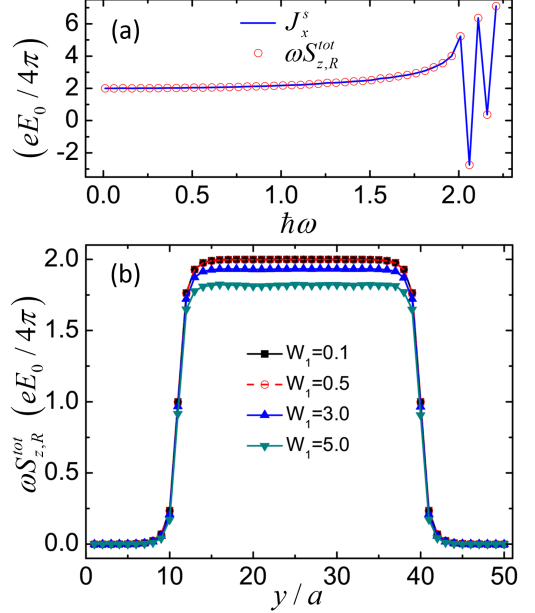


FIG. 3: (a) Spin accumulation rate $\omega S_{z,R}^{tot}(y)$ and spin current density $J_x^s(\frac{Na}{2}, y)$ at $y = \frac{Na}{2}$ as functions of frequency. (b) Spin accumulation rate $\omega S_{z,R}^{tot}(y)$ as a function of y/a for some different magnetic disorder strengths with nonmagnetic disorder strength set to $W_0 = 0$. Each data point is averaged over 300 disorder configurations. The other parameters are the same as in Fig. 2.

We wish to point out that the value $\hbar\omega = 0.05$ of the frequency set in the above calculations is already very small compared with the band gap 2. We have also studied the cases for even much smaller frequencies, e.g., $\hbar\omega = 0.001, 0.0001$, and the transverse profile of the spin current is almost unchanged. This means that the discontinuities in the spin current near the edges of the biased region will persist in the limit $\omega \rightarrow 0$, which is essentially different from the DC regime. In the DC regime, $\frac{\partial \rho_s}{\partial t} = 0$ in a steady state, so the spin current must be continuous throughout the sample. In fact, the DC regime has been known to be singular for a long time [21]. The vector potential of an exactly static electric field $E_0 \hat{y}$ may be chosen to be $-E_0 t \hat{y}$, which is unbounded and can not be treated within the Kubo linear-response theory. To overcome this difficulty, the DC regime is usually regarded as being equivalent to the $\omega \rightarrow 0$ limit of the AC regime [21]. This assumption is however not necessarily valid always. The characteristics of the transient-state spin current and spin accumulations at small frequencies revealed in this work is not extensible to the steady state in the DC regime at $\omega = 0$.

To further show quantitatively that the calculated results conform the spin conservation law, we readily derive from Eq. (3) for the following relations between the spin

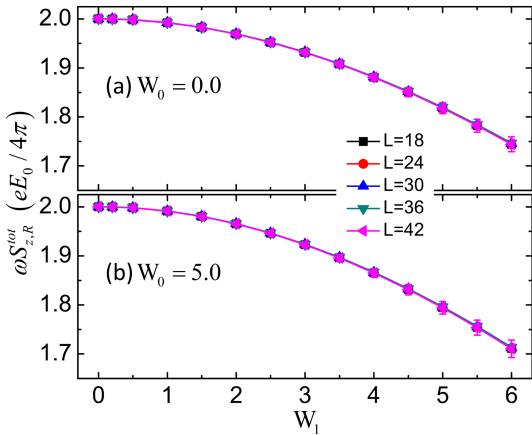


FIG. 4: Spin accumulation rate $\omega S_{z,R}^{tot}(\frac{N_a}{2})$ as a function of magnetic disorder strength, for size of the biased region ranging from $L = 18$ to 42 . The size of sample is set to $N = L + 2 \times 10$. The nonmagnetic disorder strength is chosen to be (a) $W_0 = 0$ and (b) $W_0 = 5$. Each data point is averaged over 200-500 disorder configurations.

current density and density of spin accumulation

$$\omega S_{z,R}^{tot}(y) \equiv \omega \int_{\frac{N_a}{2}}^{N_a} S_z(x, y) dx = J_x^s(\frac{N_a}{2}, y), \quad (5)$$

$$\omega S_{z,L}^{tot}(y) \equiv \omega \int_{-\frac{N_a}{2}}^{0} S_z(x, y) dx = -J_x^s(\frac{N_a}{2}, y). \quad (6)$$

Here, we have taken into account the fact that the spin current density essentially vanishes at the sample edges, i.e., $J_x^s(0, y) = J_x^s(N_a, y) = 0$, as can be seen from Fig. 2(a). Apparently, $S_{z,R}^{tot}(y)$ and $S_{z,L}^{tot}(y)$ are the total spin accumulations per unit width (in the y direction) around the right and left edges of the biased region, respectively. The quantities $\omega S_{z,R}^{tot}(y)$ and $\omega S_{z,L}^{tot}(y)$ essentially measure the changing rates of the total spin accumulations. Since $S_{z,L}^{tot}(y) = -S_{z,R}^{tot}(y)$, we will consider $S_{z,R}^{tot}(y)$ only. In Fig. 2(d), both $\omega S_{z,R}^{tot}(y)$ and $J_x^s(\frac{N_a}{2}, y)$ are plotted as functions of y . The two curves coincide with each other. In Fig. 3(a), the spin accumulation rate $\omega S_{z,R}^{tot}(y)$ and spin current density $J_x^s(\frac{N_a}{2}, y)$ at $y = \frac{N_a}{2}$ are displayed as functions of frequency, which again coincide with each other. These results are in good agreement with Eq. (5). From Fig. 3(a), we also see that at low frequencies, $J_x^s(\frac{N_a}{2}, \frac{N_a}{2})$ as well as $\omega S_{z,R}^{tot}(\frac{N_a}{2})$, divided by E_0 , are quantized to $2(\frac{e}{4\pi})$, but obvious deviations from the quantized value are observed at large frequencies. Oscillations occur when the frequency $\hbar\omega$ exceeds the band gap 2.

In order to demonstrate the robustness of the AC QSH effect, we introduce a generalized version of the Anderson disorder into the system. The total Hamiltonian of the system is then given by $H = H_0 + U$ with

$$U = \sum_{\mathbf{r}} c_{\mathbf{r}}^\dagger \left(w_{\mathbf{r}}^{(0)} + w_{\mathbf{r}}^{(1)} \mathbf{s} \cdot \mathbf{m}_{\mathbf{r}} \right) c_{\mathbf{r}}, \quad (7)$$

where $w_{\mathbf{r}}^{(0)}$ represents on-site nonmagnetic disorder, uniformly distributed in the interval $w_{\mathbf{r}}^{(0)} \in [-\frac{W_0}{2}, \frac{W_0}{2}]$, $w_{\mathbf{r}}^{(1)}$ stands for on-site magnetic disorder, distributed between $w_{\mathbf{r}}^{(1)} \in [-\frac{W_1}{2}, \frac{W_1}{2}]$, and $\mathbf{m}_{\mathbf{r}}$ is a randomly oriented unit vector. Apparently, the presence of the magnetic disorder destroys both the spin conservation and TR symmetry of the system. It is well-known that the spin current density is ill-defined in the absence of spin conservation. Nonetheless, from the above discussions, we know that the spin accumulation rate $\omega S_{z,R}^{tot}(y)$ is equivalent to the spin current density, which remains well-defined. The Kubo formula Eq. (4) is general and still valid in the presence of disorder. In Fig. 3(b), the spin accumulation rate calculated from Eq. (4) is plotted as a function of y/a for several different strengths of magnetic disorder with nonmagnetic disorder strength set to $W_0 = 0$, where each data point is averaged over 300 disorder configurations. We see that even intermediately strong magnetic disorder only suppresses the spin accumulations slightly.

We also carry out scaling analysis to study if the AC QSH effect remains stable for large samples. The calculated $\omega S_{z,R}^{tot}(\frac{N_a}{2})$ for size La of the biased region ranging from $18a$ to $42a$ is displayed as a function of magnetic disorder strength W_1 . The nonmagnetic disorder strength is set to $W_0 = 0$ and 5 in Figs. 4(a) and 4(b), respectively. In all calculations, the distance from the biased region to sample edges is fixed at $10a$. From the figures, we observe that while intermediately strong disorder suppresses the spin accumulations slightly, the spin accumulations do not decrease with increasing the sample size. Thus, we can expect that the AC QSH effect will stay stable for very large samples.

In summary, we have shown that while both the DC and AC QSH effects originate from the nontrivial bulk band topology of the two-dimensional TIs, they exhibit quite different characteristics. The DC QSH effect must be carried by the symmetry-protected edge states. The AC QSH effect can occur in the bulk without involving the fragile edge states, hence being robust against symmetry breaking and disorder. Based upon the AC QSH effect, an array of asynchronized electrical spin polarization generators can be built on a single film of QSH material, which is very beneficial for designing and fabricating spintronic integrated circuits. Moreover, the low-frequency AC QSH effect provides a relatively easy way to experimentally investigate the unconventional topological invariant underlying the QSH systems directly, compared with previous theoretical proposals, including topological magnetoelectric effect [22, 23] and topological spin pumping [24].

This work was supported by the State Key Program for Basic Researches of China under grants numbers 2015CB921202 and 2014CB921103 (L.S.), the National Natural Science Foundation of China under grant numbers 11225420 (L.S.), and a project funded by the

PAPD of Jiangsu Higher Education Institutions (L.S. and D.Y.X.). This work was also supported by the U.S. Department of Energy, Office of Basic Energy Sciences under Grant No. DE-FG02-06ER46305 (D.N.S).

W.Y.D. and H.G. contributed equally to this work.

* Electronic address: shengli@nju.edu.cn

- [1] C. L. Kane and E. J. Mele, *Phys. Rev. Lett.* **95**, 226801 (2005).
- [2] B. A. Bernevig and S. C. Zhang, *Phys. Rev. Lett.* **96**, 106802 (2006).
- [3] C. Wu, B. A. Bernevig, and S.-C. Zhang, *Phys. Rev. Lett.* **96**, 106401 (2006).
- [4] J. E. Moore and L. Balents, *Phys. Rev. B* **75**, 121306(R) (2007).
- [5] L. Fu and C. L. Kane, *Phys. Rev. B* **76**, 045302 (2007); L. Fu, C. L. Kane, and E. J. Mele, *Phys. Rev. Lett.* **98**, 106803 (2007).
- [6] H. J. Zhang, C. X. Liu, X. L. Qi, X. Dai, Z. Fang, and S. C. Zhang, *Nature Phys.* **5**, 438 (2009).
- [7] M. Z. Hasan and C. L. Kane, *Rev. Mod. Phys.* **82**, 3045 (2010).
- [8] X. L. Qi and S. C. Zhang, *Physics Today* **63**, 33 (2010).
- [9] Y. Ando, *J. Phys. Soc. Japan* **82**, 102001 (2013).
- [10] J. E. Moore, *Nat. Phys.* **11**, 897 (2015).
- [11] H. Weng, R. Yu, X. Hu, X. Dai, and Z. Fang, *Adv. Phys.* **64**, 227 (2015).
- [12] C. L. Kane and E. J. Mele, *Phys. Rev. Lett.* **95**, 146802 (2005).
- [13] D. N. Sheng, Z. Y. Weng, L. Sheng, and F. D. M. Haldane, *Phys. Rev. Lett.* **97**, 036808 (2006).
- [14] E. Prodan, *Phys. Rev. B* **80**, 125327 (2009); E. Prodan, *New J. Phys.* **12**, 065003 (2010).
- [15] H. C. Li, L. Sheng, D. N. Sheng, and D. Y. Xing, *Phys. Rev. B* **82**, 165104 (2010); Y. Yang, Z. Xu, L. Sheng, B. Wang, D. Y. Xing, and D. N. Sheng *Phys. Rev. Lett.* **107**, 066602 (2011).
- [16] M. König, S. Wiedmann, C. Brüne, A. Roth, H. Buhmann, L. W. Molenkamp, X.-L. Qi, and S.-C. Zhang, *Science* **318**, 766 (2007).
- [17] I. Knez and R.-R. Du, *Frontiers of Phys.* **7**, 200 (2012).
- [18] D. Wei, M. Obstbaum, M. Ribow, C. H. Back and G. Woltersdorf, *Nature Comm.* **5**, 3768 (2014).
- [19] B. A. Bernevig, T. L. Hughes, and S. C. Zhang, *Science* **314**, 1757 (2006).
- [20] H. Li, L. Sheng, R. Shen, L. B. Shao, B. Wang, D. N. Sheng, and D. Y. Xing, *Phys. Rev. Lett.* **110**, 266802 (2013).
- [21] Many-particle Physics, G. D. Mahan (Plenum, 1993).
- [22] X. L. Qi, T. Hughes, and S.-C. Zhang, *Phys. Rev. B* **78**, 195424 (2008).
- [23] A. M. Essin, J. E. Moore, and D. Vanderbilt, *Phys. Rev. Lett.* **102**, 146805 (2009).
- [24] M. N. Chen, L. Sheng, R. Shen, D. N. Sheng, and D. Y. Xing, *Phys. Rev. B* **91**, 125117 (2015).